Hindawi
Mobile Information Systems
Volume 2023, Article ID 9916531, 12 pages
https://doi.org/10.1155/2023/9916531

Research Article

An Underwater Target Tracking Algorithm Based on Extended Kalman Filter

Jian Huang

Communication and Countermeasures Division, Sichuan Jiuzhou Electric Group Co. Ltd, Mianyang 621000, China

Correspondence should be addressed to Jian Huang; hj.steven@163.com

Received 4 June 2022; Revised 8 September 2022; Accepted 29 September 2022; Published 3 May 2023

Academic Editor: Wang Wenyong

The technology of ocean monitoring is more advanced while the continuous development of industrial Internet. Unmanned underwater vehicle (UUV) is one of major ways for underwater environment monitoring, which makes high-precision positioning, and tracking of it is one of the key problems and needs to be solved urgently. An underwater acoustic positioning and tracking algorithm based on multiple beacons is proposed to reduce the positioning error of underwater acoustic positioning system caused by uncertain sound speed. The system consists of multiple GPS intelligent buoys floated on the sea surface and acoustic signal generator installed on the UUV. The effective sound speeds between the UUV and different buoys are considered to be unequal and estimated as the state parameters, together with the kinematic parameters of the UUV. Based on the kinematic equations of the UUV, the tracking model is obtained under the framework of the extended Kalman filter. Simulation results show that the proposed algorithm can correct the sound speed and improve the stability and accuracy of underwater acoustic positioning system.

1. Introduction

In the context of the continuous development of industrial Internet, the development of ocean monitoring in the direction of information construction has become inevitable. Due to its wide range of activities, small size, low cost, and many other advantages, unmanned underwater vehicle (UUV) has many important applications in ocean monitoring. In order to ensure the completion of underwater missions and to obtain accurate underwater measurement data, the system is required to obtain accurate position information of the UUV. Therefore, UUV's high-precision positioning and tracking is one of the key technologies for ocean monitoring.

The fact that electromagnetic signals are severely attenuated in water makes GPS hardly used for underwater positioning; however, the good propagation characteristics of sound waves make acoustic positioning an effective alternative. The underwater acoustic positioning system (UAPS) provides position information for underwater target without cumulative errors is an effective underwater positioning method. Classical UAPS includes long baseline (LBL) system [1], short baseline (SBL) system [2], and ultrashort baseline (USBL) system [3, 4].

The error source of UAPS mainly consists of four factors: the calibration error of hydrophones, the propagation time estimation error, the sound speed error, and the random error, where the most damaging error source in LBL system is the sound speed error. In previous studies, sound speed correction techniques usually use the ray acoustics theory to trace the propagation path of acoustic signal, and the straight distance is calculated from the measured propagation time on the basis of the accurately measured sound speed profile (SSP) [5–7]. In order to reduce the impact of sound speed errors on positioning, most researchers usually use different techniques to measure the SSP. However, there is an unavoidable error in the SSP measured by sound velocity profiler (SVP) or derived from conductivity, temperature, and density (CTD) measurements [8]. In addition, SSP in a certain area will also change slowly over time. All these will unfortunately lead to the degradation of sound speed correction techniques based on fixed SSP. In other sound speed

correction algorithms, there are some studies [9, 10] considered the sound speed as an unknown variable and solved the effective sound speed (ESS) in the course of positioning. However, the ESS between each hydrophone in the LBL system to the target is regarded as equal, which is very discrepant from the reality.

Experts and scholars have already done a lot of other researches on underwater acoustic positioning technology. Combining different kinds of traditional UAPSs can provide positioning redundancy and take advantages of each system, the most common of which is the USBL/LBL system [11, 12]. Xu et al. [13] first proposed the application of the difference method to underwater acoustic positioning, where the proposed single-difference method can eliminate long-term systematic errors, and the double-difference method can almost completely eliminate all system errors that depend on depth and space. In [14], a multifunctional system that combines rigidly mounted "fixed" USBL transceivers placed under water surface and "free" cable-mounted LBL stations deployed at a relatively large depth. Moreover, each baseline transponder is equipped with a high-speed communication device to provide a real-time control link for underwater vehicles and navigate them based on the current positioning data.

In UAPS, the Kalman filter (KF) is a commonly used technique to reduce system positioning errors. De Palma et al. [15] measure the distance between a single beacon and the target and locate the target by KF or the extended Kalman filter (EKF). In [10], an unscented Kalman filter (UKF) algorithm based on uncertain least squares (ULS) is proposed for underwater target positioning in moving long baseline systems, under the premise that the underwater sound speed is unknown. In the integrated navigation system, KF is also commonly used to compensate the position information provided by the UAPS to the position information provided by the inertial navigation system [16] or dead reckoning system [17], thereby, eliminating the cumulative error of the latter two systems. In [18], the integration of an USBL acoustic modem and positioning device in a two-parallel EKF multisensory navigation schema for an autonomous underwater vehicle (AUV) is presented. In [19], a constrained form of a square-root unscented Kalman filter (SRUKF) is developed, where the sigma points of the unscented transformation are projected onto the feasible region by solving constrained optimization problems.

In UAPS, the measured values of time of arrival (TOA) or time difference of arrival (TDOA) to the target are usually used to calculate the distance and bearing angle, while in the tightly coupled INS/UAPS integrated navigation system, the distance measurement value is also used as the measurement vector. Such processes usually do not take into account the refraction and multipath effects and assume that the sound speed is a known constant. Other researches [2, 9, 10] regard the underwater sound speed as an unknown variable and estimate it while positioning. However, this kind of method treats the sound speed between the target and different hydrophones as equal, which is an unrealistic assumption. Considering that the uncertain sound speed is one of the serious factors causing underwater acoustic positioning error, this paper proposes a multibeacon based UUV tracking system. The effective sound speed (ESS) between the UUV and different beacons is considered to be unequal and estimated as the state parameters, together with the kinematic parameters of the UUV. The acoustic signal propagation time between the UUV and each beacon is taken as the measurement vector, and the tracking model of UUV is obtained under the framework of EKF. Simulation experiments show that the proposed algorithm is able to correct the sound speed and improve the accuracy and stability of UAPS.

2. GPS Intelligent Buoy System and Geometric Positioning Principle of LBL System

The GPS intelligent buoy (GIB) system [20, 21] consists of several buoys equipped with GPS receivers and submerged hydrophones at the sea surface. The GIB can obtain its own absolute position information through the GPS signal. The UUV carries an acoustic signal generator that periodically broadcasts the acoustic signal. This period is determined by a high precision clock synchronized with the GPS prior to system deployment. Each hydrophone receives acoustic signals and records their arrival time with different latencies. Through the spread spectrum acoustic communication technology, the depth information of the UUV measured by itself can be transmitted to the buoys. The buoy communicates via radio with the central station, where the position of the UUV can be calculated.

The GIB system is depicted in Figure 1. The coordinate system is defined as follows: the north east down (NED) is established by selecting a point in the polygon area surrounded by the N buoys as the origin $O(0, 0, 0)$. The UUV's coordinate is $T(x, y, z)$, and the coordinates of the hydrophones on each buoy are $GIB_1(x_1, y_1, z_1), \cdots, GIB_N(x_N, y_N, z_N)$, respectively. The distances between the GIBs and the UUV are defined as $R_1, \cdots, R_N$.

In each time period, the acoustic signal generator broadcasts a signal. Since each buoy is time synchronized with the UUV, they can calculate the propagation time after receiving the acoustic signal. Multiply the propagation time by the sound speed can obtain the relative distance between the UUV and each buoy:

$$R_i = \overline{c}_i \cdot t_i, \tag{1}$$

where $\overline{c}_i$ represents the average sound speed, t_i is the propagation time of acoustic signal from the UUV to the i-th buoy, and R_i is the slant range between them. $i = 1, ..., N$ are the identification of the buoy, and N is the number of buoys.

After measuring the distance between the UUV and the buoy, the 3-D spatial relationship between them can be expressed as follows:

$$R_i^2 = (x - x_i)^2 + (y - y_i)^2 + (z - z_i)^2. \tag{2}$$

Since the distance between the buoy and the UUV is usually from a few hundred meters to tens of kilometers. Therefore, it can be assumed that the buoys are at the same horizontal plane, which can be expressed as follows:

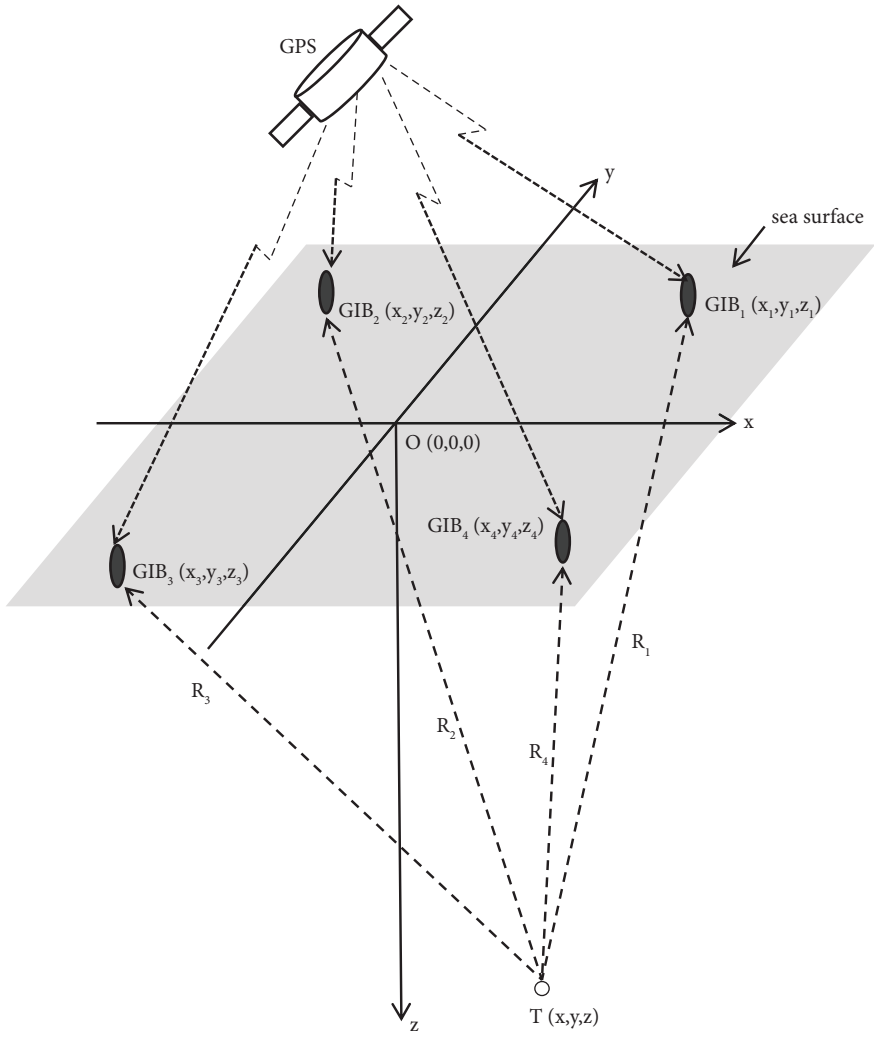

Figure 1: GIB system.

$$z - z_i = z - z_j; i \neq j. \tag{3}$$

Subtracting the equations established by two different buoys can eliminate the quadratic term of the unknown variables, resulting in the following simplified form:

$$\begin{aligned} &x_i^2 + y_i^2 - x_j^2 - y_j^2 - 2\left(x_i - x_j\right)x - 2\left(y_i - y_j\right)y \\ &= \left(\overline{c}_i t_i\right)^2 - \left(\overline{c}_j t_j\right)^2. \end{aligned} \tag{4}$$

Under the premise that the sound speed is known, the geometric positioning model of the LBL system can be described as the following function:

$$\begin{aligned} f_{i,j}(x, y) = {} & 2\left(x_i - x_j\right)x + 2\left(y_i - y_j\right)y \\ & + \left(\overline{c}_i t_i\right)^2 - \left(\overline{c}_j t_j\right)^2 - x_i^2 - y_i^2 + x_j^2 + y_j^2. \end{aligned} \tag{5}$$

Define $\widehat{x}$ and $\widehat{y}$ are the estimation of the UUV's coordinates x and y. We can calculate them by the least square (LS) method:

$$(\widehat{x}, \widehat{y}) = \operatorname{argmin} \sum_{\substack{i,j=1 \\ i \neq j}}^{N} \left[f_{i,j}(x, y)\right]^2. \tag{6}$$

After obtaining $\widehat{x}$ and $\widehat{y}$, the coordinate z of the UUV can be calculated by substituting $\widehat{x}$ and $\widehat{y}$ into (2).

2.1. Underwater Target Tracking Algorithm Based on EKF. When UUV performs underwater surveying or other works, it usually maintains a certain depth and horizontal attitude while performing target detection and information collection by changing its heading angle. Therefore, the 3-D motion of the UUV can be simplified to 2-D form [22], and the depth information of the UUV can be accurately measured by the depth sensor and transmitted to GIBs through the spread spectrum acoustic communication technology. To simplify the description, we limit the movement of the UUV in a plane at a known depth where

$z = z_o$, but the derived solution in this paper can be easily extended to the case where the UUV moves in 3-D space.

2.2. Process Model. In the process of establishing the UUV's kinematic equation, we assume that the coordinates of the UUV are (x, y), the UUV moves at a constant speed V, the angle between V and the x axis is φ, and the derivative of φ is r. The transmitted acoustic signal contains a time stamp $t_k = kh, k \in Z_+$, where h is the emission period of the acoustic signal. After GIBs receiving the signal and transmitting it to the central station, the central station uses the signals with the same time stamp to track the UUV. The discrete time kinematics model of the UUV is expressed as follows:

$$\begin{cases} x(k+1) = x(k) + hV(k)\cos(\varphi(k)), \\ y(k+1) = y(k) + hV(k)\sin(\varphi(k)), \\ V(k+1) = V(k) + \omega_V(k), \\ \varphi(k+1) = \varphi(k) + hr(k) + \omega_\varphi(k), \\ r(k+1) = r(k) + \omega_r(k), \end{cases} \tag{7}$$

where the process noise $\omega_V(k)$, $\omega_\varphi(k)$, and $\omega_r(k)$ are stationary, independent, zero-mean, and Gaussian, with constant standard deviations.

The ESS is defined as the ratio of the slant range between the transmitter and the receiver to the propagation time of the fastest arriving acoustic ray. Yang et al. [9] pointed out that the ESS is related to the spatial relationship (horizontal distance, depth difference, etc.) of the transmitter and receiver. Thus, we consider the ESS between the UUV and each GIB to be unequal since the distance between them is not equal. At the same time, we assume that the ESS keeps equal during the emission interval since the distance the UUV moves during the emission interval of the acoustic signal is much smaller than the slant range between the UUV and GIBs. In this paper, the ESSs between the UUV and each GIB are taken as the state parameter, which are estimated while tracking. Let c_i represents the ESS between the UUV and the i-th GIB, and then, we have

$$c_i(k+1) = c_i(k) + \omega_{c_i}(k); i = 1, ..., N, \tag{8}$$

where the process noise $\omega_{c_i}(k)$ is stationary, independent, zero-mean, and Gaussian, with constant standard deviations.

The above kinematic equation can be written as a linear parameter variation system model:

$$\begin{aligned} \mathbf{X}(k+1) &= f(\mathbf{X}(k)) + \mathbf{w}(k) \\ &= \mathbf{A}(\mathbf{X}(\mathbf{k})) \cdot \mathbf{X}(k) + \mathbf{L} \cdot \boldsymbol{\omega}(k), \end{aligned} \tag{9}$$

where $\mathbf{X}$ is the state vector, $\mathbf{A}$ is the transfer matrix for state, $\mathbf{L}$ is the transfer matrix for process noise, and ω is the process noise. From (7) and (8), we can obtain

$$\begin{aligned} \mathbf{X}(k) &= \left[x(k), y(k), V(k), \varphi(k), r(k), c_1(k), ..., c_N(k)\right]^T, \\ \boldsymbol{\omega}(k) &= \left[\omega_V(k), \omega_\varphi(k), \omega_r(k), \omega_{c_1}(k), ..., \omega_{c_N}(k)\right]^T, \\ \mathbf{A}(\mathbf{X}(k)) &= \begin{bmatrix} \mathbf{A}_1(\mathbf{X}(k)) & \mathbf{0}_{5\times N} \\ \mathbf{0}_{N\times 5} & \mathbf{I}_{N\times N} \end{bmatrix}, \\ \mathbf{A}_1(\mathbf{X}(k)) &= \begin{bmatrix} 1 & 0 & h\cos(\varphi(k)) & 0 & 0 \\ 0 & 1 & h\sin(\varphi(k)) & 0 & 0 \\ 0 & 0 & 1 & 0 & 0 \\ 0 & 0 & 0 & 1 & h \\ 0 & 0 & 0 & 0 & 1 \end{bmatrix}, \\ \mathbf{L} &= \begin{bmatrix} \mathbf{0}_{2\times(3+N)} \\ \mathbf{I}_{(3+N)\times(3+N)} \end{bmatrix}, \end{aligned} \tag{10}$$

and the process noise covariance is

$$\begin{aligned} \mathbf{Q} &= E\left[\boldsymbol{\omega}(k)\boldsymbol{\omega}^T(k)\right] \\ &= \mathrm{diag}\left\{\left[\sigma_V^2, \sigma_\varphi^2, \sigma_r^2, \sigma_{c_1}^2, ..., \sigma_{c_N}^2\right]^T\right\}. \end{aligned} \tag{11}$$

2.3. Measurement Model. In the calculation process, the measurement is the only connection between KF and the external environment. Whether the filter is polluted or not mainly depends on the accuracy of the input measurement information. Due to the influence of the external environment, the inaccurate sound speed estimation usually introduces a large error to the UAPS. Here, we take the acoustic signal propagation time between the UUV and each GIB as the measurement. Then, the measurement equation is

$$\mathbf{Z}(k) = h(\mathbf{X}(k)) + \mathbf{v}(k), \tag{12}$$

where $\mathbf{Z}$ is the measurement vector that satisfies the following form:

$$\mathbf{Z}(k) = \left[z_1(k), \ldots, z_N(k)\right]^T, \tag{13}$$

where $z_i(k)$ is the propagation time of the acoustic signal between the UUV and the i-th GIB at step k:

$$z_i(k) = \frac{1}{c_i(k)} \sqrt{\left(x_i - x(k)\right)^2 + \left(y_i - y(k)\right)^2 + \left(z_i - z_o\right)^2} + v_i(k); i = 1, \ldots, N, \tag{14}$$

where the measurement noise $v_i(k)$ is stationary, independent, zero-mean, and Gaussian, with constant standard deviations, and the measurement noise covariance is

$$\begin{aligned} \mathbf{R} &= E\left[\mathbf{v}(k)\mathbf{v}^T(k)\right] \\ &= \operatorname{diag}\left\{\left[\sigma_{v_1}^2, \ldots, \sigma_{v_N}^2\right]^T\right\}. \end{aligned} \tag{15}$$

2.4. Design of EKF. The algorithm adopts the basic equation of the standard EKF, and its time update equations are as follows:

$$\begin{aligned} \hat{\mathbf{X}}(k+1/k) &= \mathbf{F}(\hat{\mathbf{X}}(k)) \cdot \hat{\mathbf{X}}(k), \\ \mathbf{P}(k+1/k) &= \mathbf{F}(\hat{\mathbf{X}}(k)) \cdot \mathbf{P}(k) \cdot \mathbf{F}^T(\hat{\mathbf{X}}(k)) + \hat{\mathbf{L}} \cdot \mathbf{Q} \cdot \hat{\mathbf{L}}^T, \end{aligned} \tag{16}$$

where $\mathbf{P}$ is the covariance of the predicted state, and $\mathbf{F}(\hat{\mathbf{X}}(k))$ and $\hat{\mathbf{L}}$ are process Jacobians at step k:

$$\begin{aligned} \mathbf{F}(\hat{\mathbf{X}}(k)) &= \left.\frac{\partial f(\mathbf{X})}{\partial \mathbf{X}}\right|_{\hat{\mathbf{X}}(k)} \\ &= \begin{bmatrix} \mathbf{F}_1(\hat{\mathbf{X}}(k)) & \mathbf{0}_{5\times N} \\ \mathbf{0}_{N\times 5} & \mathbf{I}_{N\times N} \end{bmatrix}, \\ \hat{\mathbf{L}} &= \mathbf{L}, \end{aligned} \tag{17}$$

where

$$\mathbf{F}_1(\hat{\mathbf{X}}(k)) = \begin{bmatrix} 1 & 0 & h\cos(\hat{\varphi}(k)) & -h\hat{V}(k)\sin(\hat{\varphi}(k)) & 0 \\ 0 & 1 & h\sin(\hat{\varphi}(k)) & h\hat{V}(k)\cos(\hat{\varphi}(k)) & 0 \\ 0 & 0 & 1 & 0 & 0 \\ 0 & 0 & 0 & 1 & h \\ 0 & 0 & 0 & 0 & 1 \end{bmatrix}. \tag{18}$$

The EKF measurement update equations are as follows:

$$\begin{aligned} \mathbf{X}(k+1) &= \hat{\mathbf{X}}(k+1/k) + \mathbf{K} \cdot \left[\mathbf{Z}(k) - h(\hat{\mathbf{X}}(k+1/k))\right], \\ \mathbf{K} &= \mathbf{P}(k+1/k) \cdot \mathbf{G}^T(\hat{\mathbf{X}}(k)) \cdot \left[\mathbf{G}(\hat{\mathbf{X}}(k)) \cdot \mathbf{P}(k+1/k) \cdot \mathbf{G}^T(\hat{\mathbf{X}}(k)) + \mathbf{R}\right]^{-1}, \\ \mathbf{P}(k+1) &= \left[\mathbf{I} - \mathbf{K} \cdot \mathbf{G}(\hat{\mathbf{X}}(k))\right] \cdot \mathbf{P}(k+1/k), \end{aligned} \tag{19}$$

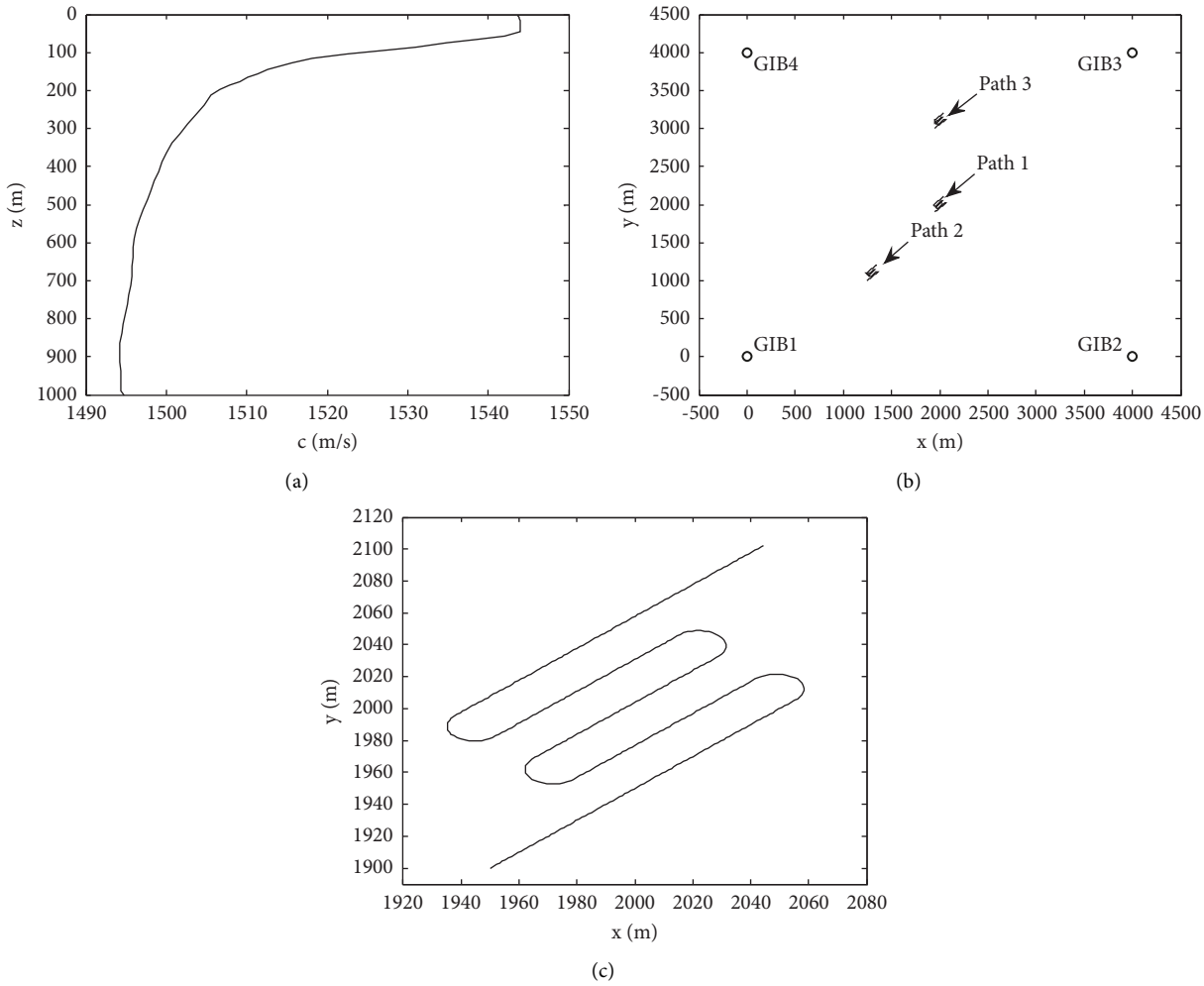

Figure 2: System configuration and the actual path: (a) sound speed profile, (b) system configuration, and (c) detail of the path.

where $\boldsymbol{K}$ is the filter gain, and $\mathbf{G}(\widehat{\mathbf{X}}(k))$ is the measurement Jacobian at step k:

$$\mathbf{G}(\widehat{\mathbf{X}}(k)) = \frac{\partial h(\widehat{\mathbf{X}}(k))}{\partial \mathbf{X}}\bigg|_{\widehat{\mathbf{X}}(k)} = \begin{bmatrix} -\frac{\left(x_1 - \widehat{x}(k)\right)}{c_1(k)\cdot R_1(k)} & -\frac{\left(y_1 - \widehat{y}(k)\right)}{c_1(k)\cdot R_1(k)} & 0\ 0\ 0 & -\frac{R_1(k)}{c_1^2(k)} & \cdots & 0 \\ -\frac{\left(x_2 - \widehat{x}(k)\right)}{c_2(k)\cdot R_2(k)} & -\frac{\left(y_2 - \widehat{y}(k)\right)}{c_2(k)\cdot R_2(k)} & 0\ 0\ 0 & 0 & -\frac{R_2(k)}{c_2^2(k)}\cdots & 0 \\ \vdots & \vdots & \vdots & \vdots & \ddots & \vdots \\ -\frac{\left(x_N - \widehat{x}(k)\right)}{c_N(k)\cdot R_N(k)} & -\frac{\left(y_N - \widehat{y}(k)\right)}{c_N(k)\cdot R_N(k)} & 0\ 0\ 0 & 0 & \cdots & -\frac{R_N(k)}{c_N^2(k)} \end{bmatrix}, \tag{20}$$

Table 1: Initial values setting.

Parameters	Initial values
$\mathbf{X}(0)$	$[\,1950\text{m}\ \ 1900\text{m}\ \ 1.5\text{m/s}\ \ \pi/4\text{rad}\ \ 0\text{rad/s}\,]^T$
$\hat{\mathbf{X}}(0)$	$[\,1970\text{m}\ \ 1880\text{m}\ \ 1.0\text{m/s}\ \ \pi/2\text{rad}\ \ 0\text{rad/s}\,]^T$
$\hat{c}_i(0)$	$1500\text{m/s}, i = 1, \ldots, 4$
$\hat{\mathbf{P}}(0)$	$\text{diag}\{[\,(20\text{m})^2\ \ (20\text{m})^2\ \ (0.5\text{m/s})^2\ \ (0.05\text{rad})^2\ \ (0.005\text{rad/s})^2\ \ (0.01\text{m/s})^2\ \cdots\ (0.01\text{m/s})^2\,]\}$
σ_V	0.001m/s
σ_φ	0.005rad
σ_r	0.02rad/s
σ_{c_i}	$0.01\text{m/s}, i = 1, \ldots, 4$
σ_{v_i}	$0.0005\text{s}, i = 1, \ldots, 4$

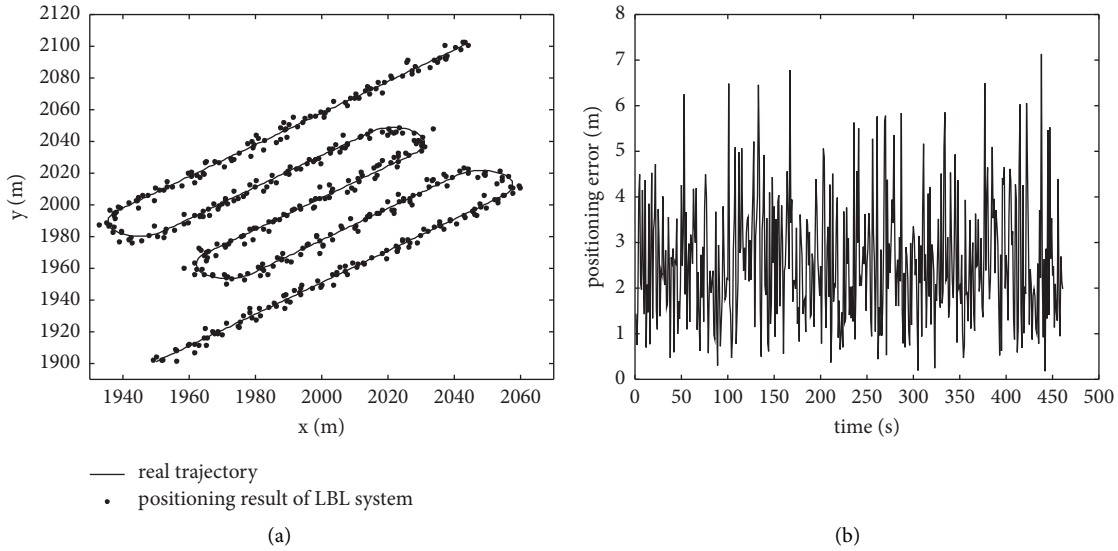

Figure 3: Positioning result of LBL system: (a) estimation path and (b) positioning error.

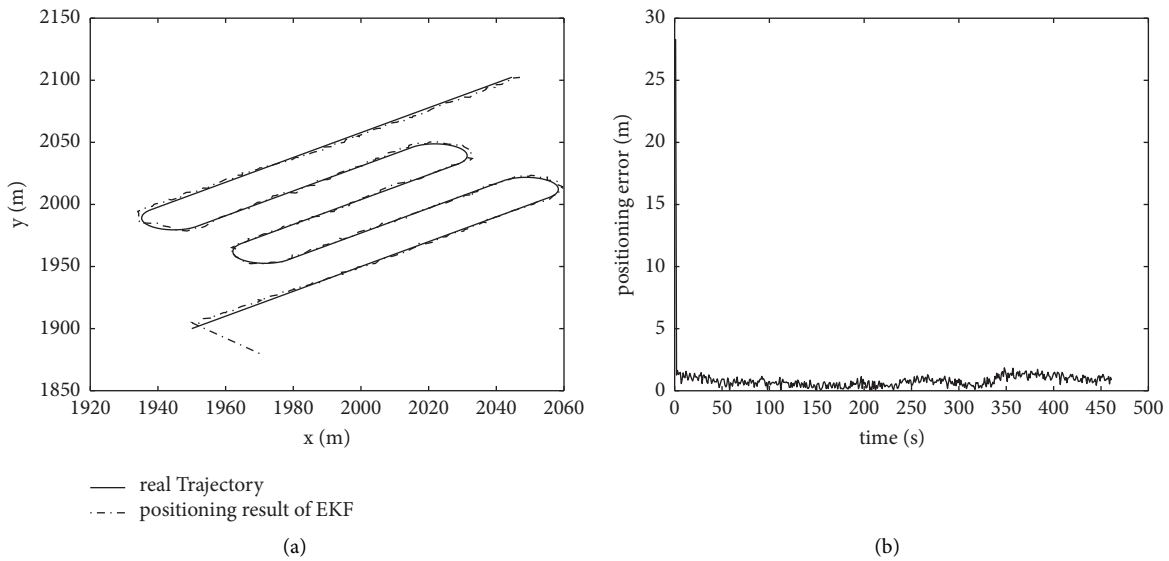

Figure 4: Positioning result of EKF-based algorithm: (a) estimation path and (b) positioning error.

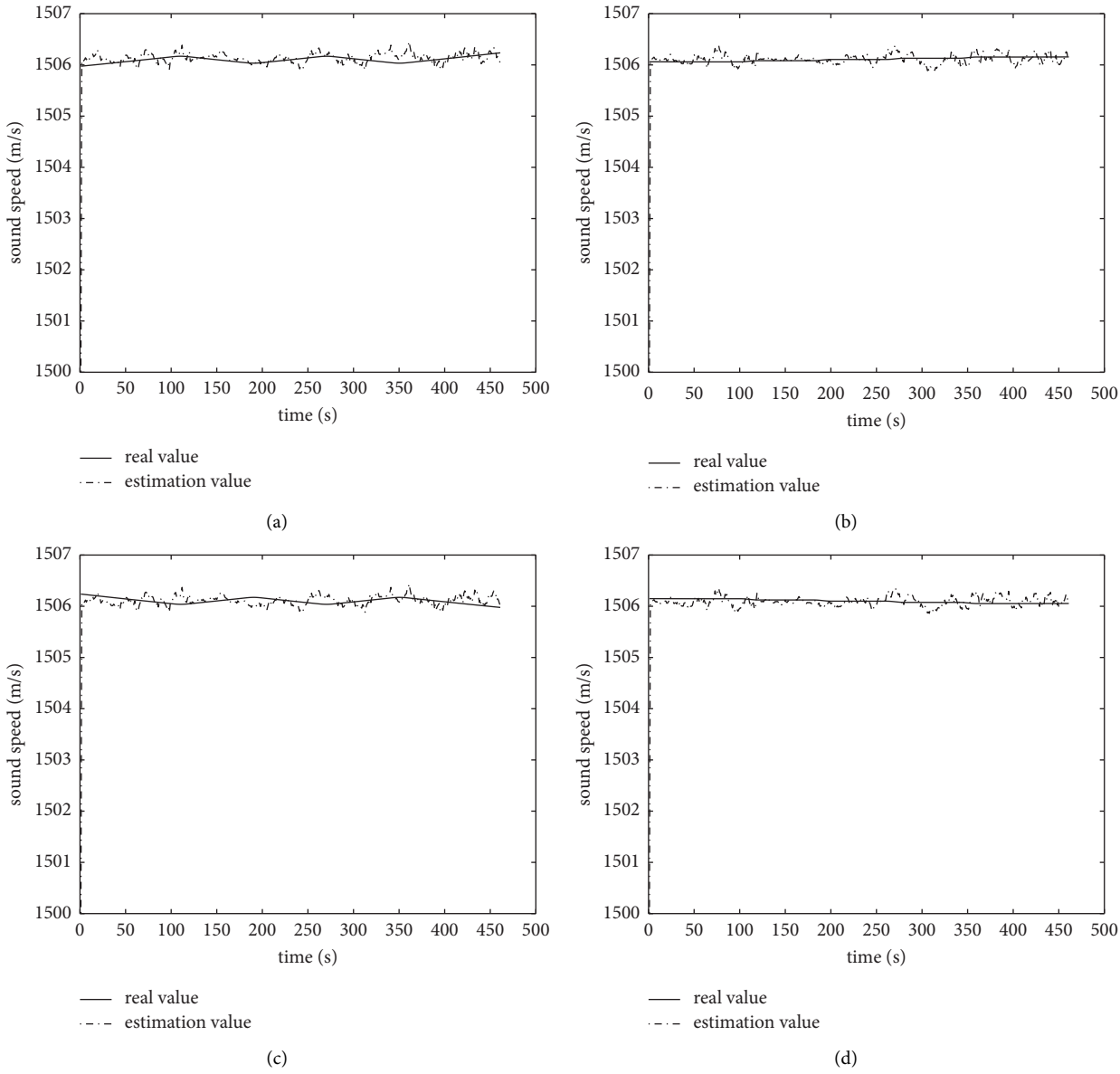

Figure 5: Estimation result of ESSs: (a) c_1, (b) c_2, (c) c_3, and (d) c_4.

where R_i is the slant range between the UUV and i-th GIB:

$$R_i(k) = \sqrt{(x_i - x(k))^2 + (y_i - y(k))^2 + (z_i - z_o)^2}. \quad (21)$$

3. Simulations

This section describes the results of simulations aimed at assessing the efficacy of the algorithms derived. The environmental file used in the simulations is the real measured data of a certain sea experiment, and the sound speed profile is depicted in Figure 2(a). The acoustic signal propagation time is obtained by the BELLHOP [23] model. As shown in Figure 2(b), the GIB system consists of four GIBs, which form a rectangle with the baseline length is 4 km. The UUV is moving at a constant speed in the plane of depth $z_0 = 800m$. Figure 2(c) shows the detail of the real path. The initial values of the EKF algorithm are given in Table 1, where the initial value of first five operating parameters is given as $\mathbf{X}(0)$.

First, we track the UUV travels along the Path 1 depicted in Figure 2(b). The emission period of the acoustic signal is $h = 1s$. It is assumed that the transmitted acoustic signals can be correctly received by all GIBs. For each acoustic signal received by the GIB, the UUV is positioned by the LBL system using geometric method and the EKF based positioning method, respectively. During the LBL positioning, the sound speed is set to 1505.29m/s as the weighted average sound speed [24] at depth 800 m of the sound speed profile as shown in Figure 2(a). The positioning results of the two methods are shown in Figures 3 and 4, respectively. For each positioning result, the distance positioning error is calculated using the following equation:

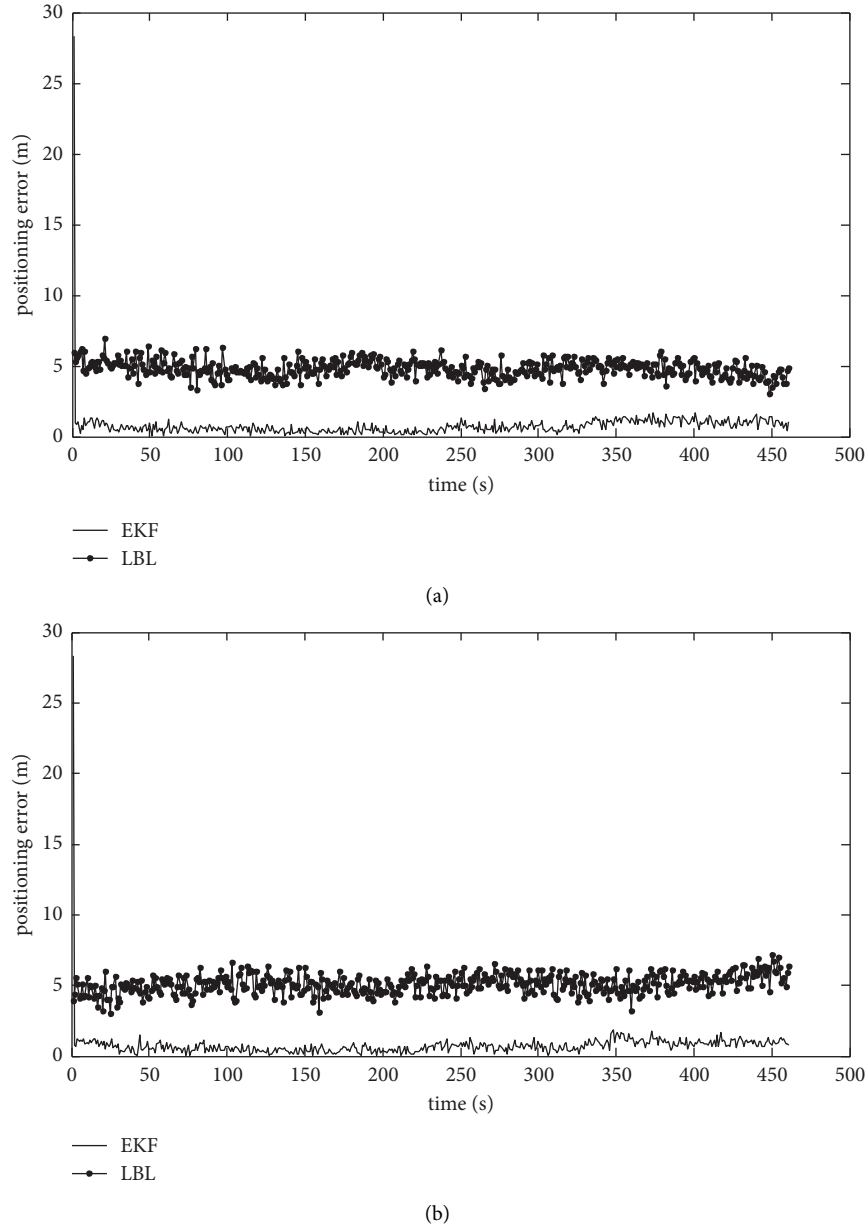

Figure 6: Positioning error of Path 2 and Path 3 by two methods: (a) Path 2 and (b) Path 3.

$$DE = \sqrt{(\hat{x} - x)^2 + (\hat{y} - y)^2}, \tag{22}$$

where (x, y) is the true coordinates of the UUV, and $(\hat{x}, \hat{y})$ is the estimation results. It can be seen that the positioning result obtained by the LBL algorithm deviates far from the real location, and the positioning result calculated by the EKF algorithm is very close to the real path, except for the error of the initial estimation. This is because the accurate sound speed cannot be obtained during the positioning of the LBL system, which results in a large positioning error. However, in the process of EKF-based algorithm, the ESS of acoustic signal propagation can be synchronously estimated (the estimation result of ESSs is shown in Figure 5), and these estimated ESS are used to track the UUV to obtain more accurate positioning result. The final distance positioning error is less than 2 m.

On the basis of the above simulation, the travel path is changed by modifying the start point of the UUV. The first two parameters of $\mathbf{X}(0)$ in Table 1 are set to (1950 m, 1000 m) (Path 2, the distances between the start point and each GIB are 1788.66 m, 3033.04 m, 4147.20 m, and 3346.54 m, respectively) and (1950 m, 3000 m) (Path 3, the distances between the start point and each GIB are 3665.97 m, 3720.12 m, 2416.47 m, and 2332.23 m, respectively). The UUV is tracking by two methods, and the obtained result is shown in Figure 6. The corresponding estimation result of ESSs is shown in Figure 7.

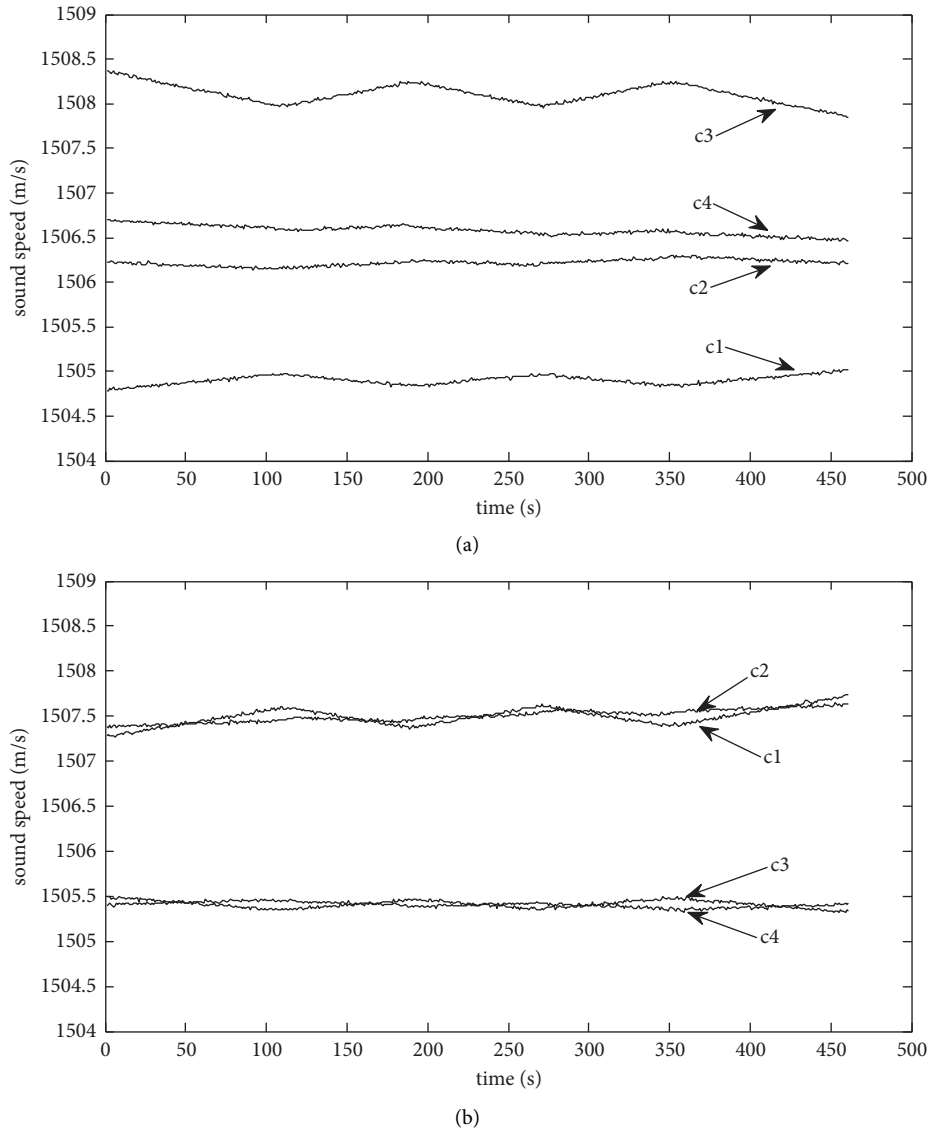

Figure 7: ESSs estimation result of Path 2 and Path 3: (a) Path 2 and (b) Path 3.

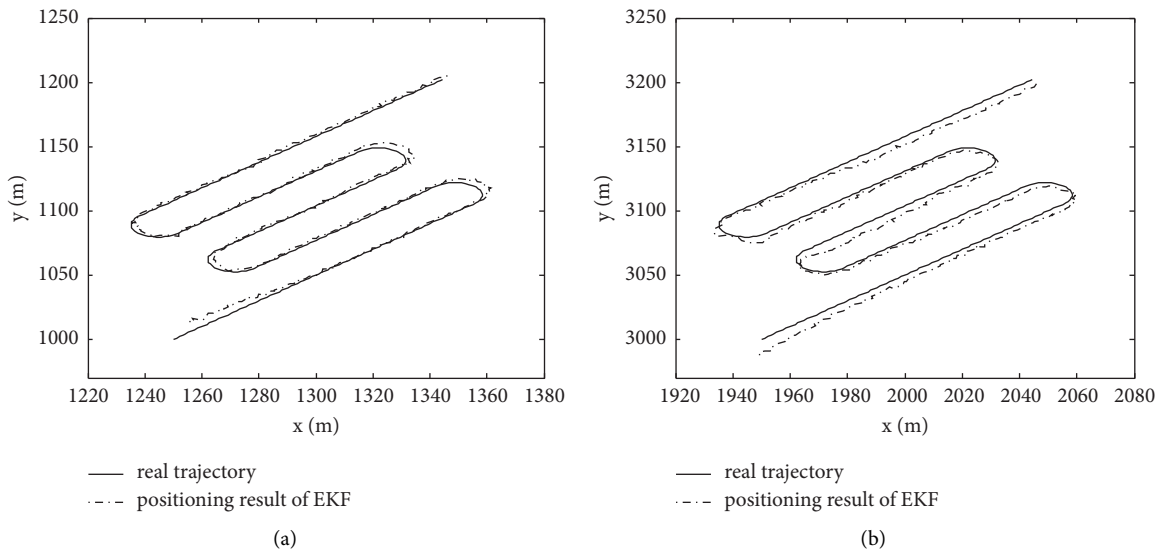

Figure 8: Tracking results of two paths assuming that the ESSs are equal: (a) Path 2 and (b) Path 3.

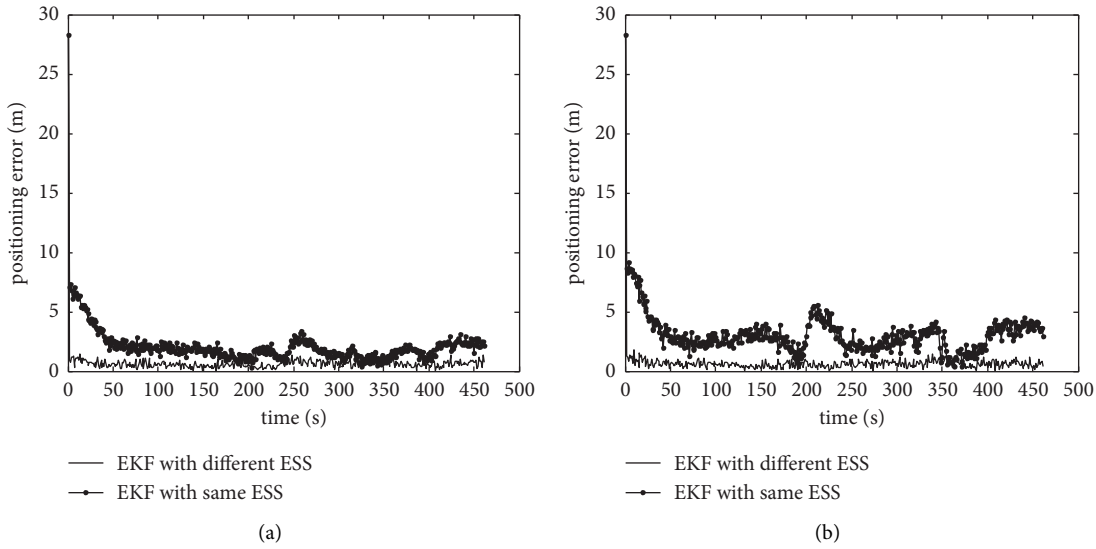

Figure 9: Position error of EKF algorithm with equal or unequal ESSs: (a) Path 2 and (b) Path 3.

For Path 1, the ESSs are almost equal since the difference of the distances between the UUV and each buoy is small. It can be clearly seen from Figure 7 that when the distances between the UUV and each GIB differ greatly, the corresponding ESSs also have a large difference, which indicates that the algorithm proposed in this paper can effectively estimate the ESS in real time. As can be seen from the positioning result from Figure 6, the LBL system cannot obtain an accurate sound speed. Using a single sound speed will cause a large positioning error, and the EKF-based algorithm estimates the ESS while the process of tracking, which can improve the positioning accuracy.

If the classical idea is used, that is, the ESSs between the UUV and different buoys are equal (i.e., $c_1 = \cdots = c_N$). The UUVs in Path 2 and Path 3 are tracked by EKF-based algorithm, and the result is depicted in Figure 8. Figure 9 shows the positioning error of the EKF-based algorithm on the UUV in these two paths, assuming that the ESSs are equal or unequal, respectively. It can be seen in both cases that the positioning results have a certain offset as a whole if a single ESS is used, especially for Path 3. This means that the positioning accuracy has some relationship with the location of the UUV if the ESSs are considered as equal. The algorithm proposed in this paper regards the ESS as unequal, so they can be estimated separately, which allows the EKF-based algorithm to achieve good performance wherever the UUV is located.

4. Conclusion

The classical geometric positioning method of UAPS usually ignores the positioning error caused by inaccurate sound speed. In this paper, an UUV positioning and tracking algorithm based on multibeacon is proposed. By setting the ESSs between the UUV and different buoys unequal, the ESSs are used as the state parameter to be estimated, and the propagation time is used as the measurement. Under the framework of EKF, the kinematics equations of the UUV are utilized, and the corresponding formulas are derived. The algorithm is verified by simulations, and the results show that the proposed algorithm can correct the sound speed estimation and improve the stability and accuracy of the UAPS. By using spread spectrum acoustic communication technology, the proposed method can be conveniently implemented in the application of underwater multitarget positioning and tracking.

Data Availability

The data supporting the current study are available from the corresponding author upon request.

Conflicts of Interest

The authors declare that they have no conflicts of interest.

Acknowledgments

This work was supported by the Science and Technology Project of Sichuan Province (2021YFG0014).

References

[1] W. Chen, W. Yan, R. Cui, and H. Cui, "Optimal configuration of USVs for moving long baseline positioning system," in *Proceedings of the International Conference on Advanced Robotics and Mechatronics*, pp. 394–398, IEEE, Macau, China, August 2016.

[2] W. Cheng, "Research for enhancing the precision of asymmetrical SBL system for any vessels," *Ocean Engineering*, vol. 33, no. 10, pp. 1271–1282, 2006.

[3] J. Reis, M. Morgado, P. Batista, P. Oliveira, and C. Silvestre, "Design and experimental validation of a USBL underwater acoustic positioning system," *Sensors*, vol. 16, no. 9, p. 1491, 2016.

[4] F. Zhong and W. Zhou, "Optimal method for USBL underwater acoustic positioning by combining TDOA and

TOA," in *Proceedings of the ACM International Conference on Underwater Networks & Systems*, no. 45, October 2016.

[5] H. Ramezani, H. Jamali-Rad, and G. Leus, "Localization and tracking of a mobile target for an isogradient sound speed profile," *IEEE International Conference on Communications*, pp. 3654–3658, 2012.

[6] H. Ramezani, H. Jamali-Rad, and G. Leus, "Target localization and tracking for an isogradient sound speed profile," *IEEE Transactions on Signal Processing*, vol. 61, no. 6, pp. 1434–1446, 2013.

[7] T. E. Barnard, F. J. Klein, and L. Resca, "Ray theory results and ray wavefront diagrams for the hyperbolic cosine propagation sound-speed profile," *IEEE Journal of Oceanic Engineering*, vol. 40, no. 4, pp. 938–946, 2015.

[8] S. Jamshidi and M. N. Abu Bakar, "An analysis on sound speed in seawater using CTD data," *Journal of Applied Sciences*, vol. 10, no. 2, pp. 132–138, 2010.

[9] F. Yang, X. Lu, J. Li, L. Han, and Z. Zheng, "Precise positioning of underwater static objects without sound speed profile," *Marine Geodesy*, vol. 34, no. 2, pp. 138–151, 2011.

[10] W. Yan, W. Chen, and R. Cui, "Moving long baseline positioning algorithm with uncertain sound speed," *Journal of Mechanical Science and Technology*, vol. 29, no. 9, pp. 3995–4002, 2015.

[11] A. Caiti, F. D. Corato, D. Fenucci et al., "Experimental results with a mixed USBL/LBL system for AUV navigation," in *Proceedings of the Underwater Communications and Networking*, pp. 1–4, IEEE, Sestri Levante, Italy, September 2015.

[12] P. Batista, C. Silvestre, and P. Oliveira, "Tightly coupled long baseline/ultra-short baseline integrated navigation system," *International Journal of Systems Science*, vol. 47, no. 8, pp. 1837–1855, 2016.

[13] P. Xu, M. Ando, and K. Tadokoro, "Precise, three-dimensional seafloor geodetic deformation measurements using difference techniques," *Earth Planets and Space*, vol. 57, no. 9, pp. 795–808, 2005.

[14] K. G. Kebkal, O. G. Kebkal, S. G. Yakovlev, and R. Bannasch, "Experimental performance of a hydro-acoustic USBL-aided LBL positioning and communication system," *IFAC Proceedings Volumes*, vol. 45, no. 5, pp. 249–254, 2012.

[15] D. De Palma, F. Arrichiello, G. Parlangeli, and G. Indiveri, "Underwater localization using single beacon measurements: observability analysis for a double integrator system," *Ocean Engineering*, vol. 142, pp. 650–665, 2017.

[16] G. T. Donovan, "Position error correction for an autonomous underwater vehicle inertial navigation system (INS) using a particle filter," *IEEE Journal of Oceanic Engineering*, vol. 37, no. 3, pp. 431–445, 2012.

[17] Y. Guo, C. Li, D. Zhang, Z. Tiehu, S. Rui, and Z. Yanshun, "The integrated navigation method by underwater towing body based on dead reckoning/hydroacoustic positioning system," *Marine Geology Frontiers*, vol. 31, no. 6, pp. 63–67, 2015.

[18] E. Guerrero-Font, M. Massot-Campos, P. L. Negre, F. Bonin-Font, and G. O. Codina, "An USBL-aided multisensor navigation system for field AUVs," in *Proceedings of the 2016 IEEE International Conference on Multisensor Fusion and Integration for Intelligent Systems (MFI)*, September 2017.

[19] S. Yousefi, X. W. Chang, and B. Champagne, "Mobile localization in non-line-of-sight using constrained square-root unscented kalman filter," *IEEE Transactions on Vehicular Technology*, vol. 64, no. 5, pp. 2071–2083, 2015.

[20] H. G. Thomas, "GIB buoys: an interface between space and depths of the oceans," in *Proceedings of the Workshop on Autonomous Underwater Vehicles*, pp. 181–184, IEEE, Cambridge, MA, USA, August 2002.

[21] A. Alcocer, P. Oliveira, and A. Pascoal, "Study and implementation of an EKF GIB-based underwater positioning system," *Control Engineering Practice*, vol. 15, no. 6, pp. 689–701, 2007.

[22] Z. Yan, S. Peng, J. Zhou, J. Xu, and H. Jia, "Research on an improved dead reckoning for AUV navigation," in *Proceedings of the Chinese Control and Decision Conference*, pp. 1793–1797, Xuzhou, China, May 2010.

[23] M. B. Porter, *The BELLHOP Manual and User's Guide: Preliminary Draft*, Heat, Light, and Sound Research, Inc, La Jolla, CA, USA, 2011.

[24] C. Yi, W. Ren, and C. Wang, "Analysis on error of secondary acoustic positioning system," *Oil Geophysical Prospecting*, vol. 44, no. 2, pp. 136–139, 2009.